Electronic Supplementary Material (ESI) for ChemComm.

Supporting Information

Hybrid ultramicroporous materials (HUMs) with enhanced stability and trace carbon capture performance

Amrit Kumar,[§†] Carol Hua,[§†] David G. Madden,[§] Daniel O'Nolan,[§] Kai-Jie Chen,[§] Lee-Ann Jane Keane,[§] John J. Perry IV,[§] Michael J. Zaworotko[*§]

[§]Bernal Institute, Department of Chemical Sciences, University of Limerick, Limerick, Republic of Ireland

† These authors contributed equally to this work.

* Contact Author, Michael.Zaworotko@ul.ie

Contents

Experimental Procedures

Zeolite 13X was obtained from Sigma-Aldrich. **SIFSIX-3-Ni**,[1] **Mg-MOF-74**,[2] **UiO-66-NH$_2$**,[3] **Ni-MOF-74**[4] and **HKUST-1**[5] were synthesised according to literature procedures.

Preparation of {[Ni(pyrazine)$_2$(TiF$_6$)]$_n$} (TIFSIX-3-Ni). Nickel hexafluorotitanate (0.500 g, 2.27 mmol) and pyrazine (2.50 g, 31.2 mmol) were dissolved in 1 mL of deionised water and stirred for 48 h at room temperature to yield an as yet uncharacterised polycrystalline precursor of **TIFSIX-3-Ni** (blue colour powder). The precursor was air dried and heated at 160 °C for 24 h to obtain the desired **TIFSIX-3-Ni**. Activation of **TIFSIX-3-Ni** was achieved by degassing the sample on a SmartVacPrep™ using dynamic vacuum and heating for 24 h (sample heated from RT to 160 °C with a ramp rate of 10 °C/min).

Preparation of {[Ni(pyrazine)$_2$(NbOF$_5$)]$_n$} (NbOFFIVE-1-Ni). The compound **NbOFFIVE-1-Ni** was synthesised and activated using a reported synthesis method.[6] Nickel nitrate hexahydrate (0.175 g, 0.602 mmol), niobium(V) oxide (0.0790 g, 0.297 mmol), pyrazine (0.384 g, 4.79 mmol) and hydrofluoric acid (0.26 mL, aqueous 48%, 7.17 mmol) were added to 3 mL of deionized water in a Teflon bomb and heated at 130 °C for 24 h . Violet coloured crystals were obtained upon cooling the reaction mixture to room temperature. The crystals obtained were washed with methanol to remove any traces of unreacted hydrofluoric acid. Activation of **NbOFFIVE-1-Ni** was carried out by degassing the methanol-washed sample on a SmartVacPrep™ using dynamic vacuum and heating for 24 h (sample heated from RT to 105 °C with a ramp rate of 10 °C/min).

Powder X-ray Diffraction (PXRD). Diffractograms were recorded using a PANalytical Empyrean™ diffractometer equipped with a PIXcel^{3D} detector operating in scanning line detector mode with an active length of 4 utilizing 255 channels. The diffractometer is outfitted with an Empyrean Cu LFF (long fine-focus) HR (9430 033 7310x) tube operated at 40 kV and 40 mA and CuKα radiation ($\lambda\alpha$ = 1.540598 Å) was used for diffraction experiments. Continuous scanning mode with the goniometer in the theta-theta orientation was used to collect the data. Incident beam optics included the Fixed Divergences slit with anti-scatter slit PreFIX module, with a 1/8° divergence slit and a 1/4° anti-scatter slit, as well as a 10 mm fixed incident beam mask and a Soller slit (0.04 rad). Divergent beam optics included a P7.5 anti-scatter slit, a Soller slit (0.04 rad), and a Ni-β filter. In a typical experiment, 20 mg of sample was dried, ground into a fine powder and was loaded on a zero background silicon disks. The data was collected from 5°- 45° (2θ) with a step-size of 0.02626° and a scan time of 29 seconds per step. Crude data was analysed using the X'Pert HighScore Plus™ software V 4.1 (PANalytical, The Netherlands). Plots of stacked PXRD spectra for each adsorbent displaying the diffraction pattern for calculated and as synthesized materials are provided below (Fig. S2-S3). Additional plots of stacked PXRD spectra displaying patterns for calculated, pristine sample, and post-humidity chamber exposure (after 1, 7, and 14 d) are provided for each sorbent. (Fig. S12 and S14)

Thermogravimetric Analysis (TGA). Thermograms were recorded under nitrogen using TGA instrument TA Q50 V20.13 Build 39. Platinum pans and a flow rate of 60 mL/min for the nitrogen gas were used for the experiments. The data was collected in the High Resolution Dynamic mode with a sensitivity of 1.0, a resolution of 4.0, and a temperature ramp of 20 °C/min up to 500 °C. The data was evaluated using the T.A. Universal Analysis suite for Windows XP/Vista Version 4.5A. Plots of stacked thermograms for each microporous sorbent are provided below (Fig. S4–S5).

Gas Sorption Measurements. Ultra-high-purity grade N_2 and CO_2 were used for gas sorption experiments. Adsorption experiments (up to 1 bar) for different pure gases were performed on Micromeritics TriStar II PLUS and Micromeritics 3 Flex surface area and pore size analyser. Measurements with N_2 at 77 K were conducted on a Micromeritics TriStar II PLUS instrument. Brunauer-Emmett-Teller (BET) surface areas were determined from the N_2 adsorption isotherms at 77 K using the Micromeritics Microactive software except for **NbOFFIVE-1-Ni** and **TIFSIX-3-Ni** whose BET surface areas were determined from the CO_2 adsorption isotherms collected at 298 K. About 200 mg of activated samples were used for the measurements. Very low pressure CO_2 measurements were performed on a Micromeritics 3 Flex surface area and pore size analyser at 273, 283, 293 and 298 K. A Julabo temperature controller was used to maintain a constant temperature in the bath through the duration of the experiment. Samples were degassed on a Smart VacPrep instrument prior to the analysis.

TGA-Temperature-Programmed Desorption (TPD) Studies. Gas mixing rig coupled independently with a TGA instrument TA Q50 V20.13 Build 39 and mass spectrometer (MS) Agilent 5975 MSD was used for the TGA-TPD studies, see Fig. S1. A typical test involved activating the sample by heating at desired temperature under a 60 mL/min flow of nitrogen gas and then cooling it down to 30 °C before the introduction of the desired gas mixture. Gas ratios was controlled and monitored by mass flow controller whereas moisture was introduced by passing the pre-mixed gas mixture through a gas bubbler containing water. Increase in weight was monitored until it began to plateau along with exposure time and gas flow conditions. Composition of the adsorbed species was analysed during the desorption cycle using the mass spectrometer. Custom-made fixed-bed flow system consisting of gas delivery system, a reactor housed in a furnace and a mass spectrometer detection system was used for the TPD experiments. Amount of guest adsorbed and the temperature at which desorption occurs can be figured out using the TPD profiles. A typical CO_2 TPD profile tells us about the amount of CO_2 adsorbed and the range of desorption temperature. It is carried out by placing the sorbent in a quartz tubular reactor and the sample is fixed within it using quartz wool. Helium is passed through the reactor until a constant signal is recorded by the mass spectrometer followed by increase in temperature at the rate of 10 °C/min to the desired temperature so as to remove the impurities. Once the impurities are flushed out, the sample is cooled down to 30 °C and the gas mixture is introduced till the desired loading is obtained. Once the desired adsorption parameters are obtained, gas flow is switched to nitrogen to flush out the excessive CO_2 in the system. Once the CO_2 concentration reaches the background levels, carrier gas is switched to helium (it is not detected by the MS, ensuring that all desorbed species from the adsorbents are detected) and the temperature of the reactor is raised at the rate of 10 °C/min. Composition of the desorbed gas was monitored by MS thus helping us to figure out the identity and quantity of each component present in the desorbed gas.

A typical direct air capture (DAC) test, involves activation of sample as per the reported conditions followed by exposure to the laboratory environment for 24 h. Analysis of the exposed sample is carried out using TPD studies to determine the composition of the adsorbed gas.

Accelerated Stability Protocol. In pharmaceutical industry, there exists a well-established criteria for the determination of a compound's stability to long-term and accelerated storage conditions.[7] The procedure incorporates all possible storage conditions from different regions around the globe. Approved as a unified testing condition by International Conference of Harmonization (ICH) it consists of long-term, intermediate and accelerated storage conditions valid for the USA, EU and Japan. Proven by Arrhenius equation to be a valid model, accelerated stability conditions mimic an acceleration of the storage at ambient conditions and accelerated stability testing for 6 months is similar to two years of long-term storage conditions.[8] In a typical experiment, pristine sample of the adsorbent under investigation was prepared and placed into an environment where relative humidity temperature and were controlled. To achieve 75% relative humidity at 40 °C, saturated aq. NaCl solution is placed in a desiccator stored at 40 °C. Adsorbents were placed in a separate, open glass vial and stored within the desiccator. They were exposed to this temperature and humidity continuously and aliquots were removed for analysis (PXRD, TGA, and gas sorption) after 1, 7, and 14 d.

Scheme of Thermogravimetric (TGA)-Temperature-Programmed Desorption (TPD).

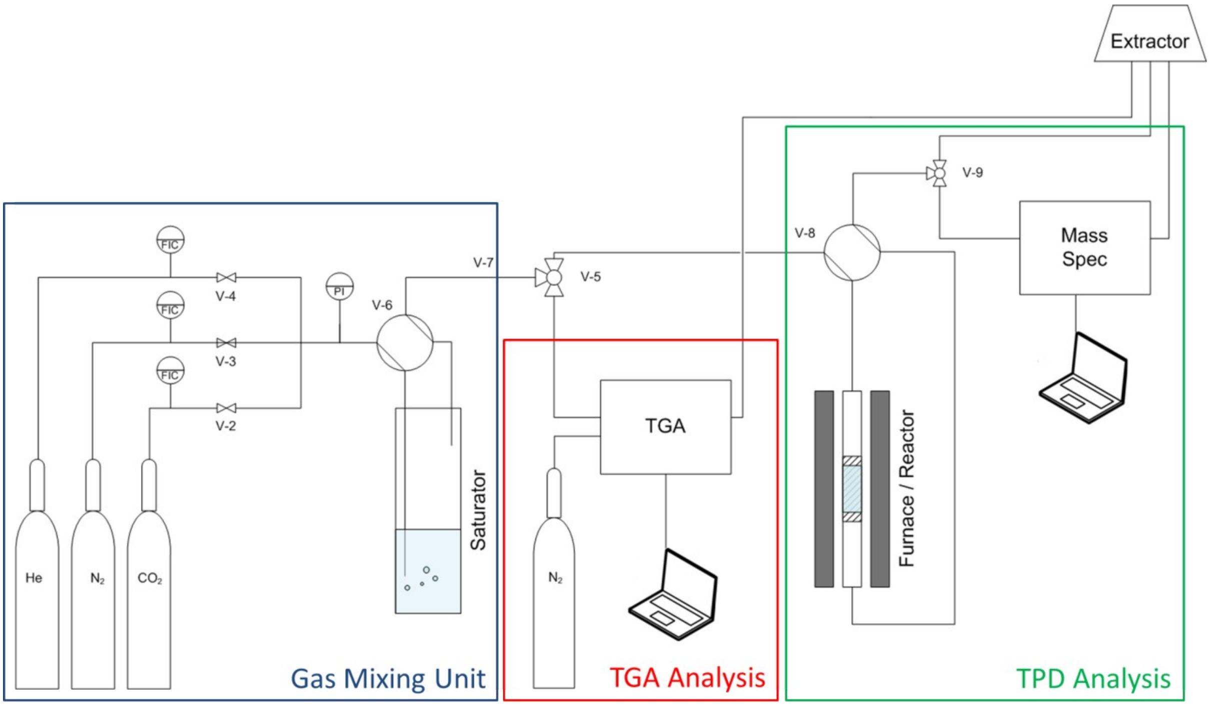

Figure S1: Schematic of gas mixing system, TGA uptake analysis and TPD analysis units.

Powder X-ray Diffraction for TIFSIX-3-Ni.

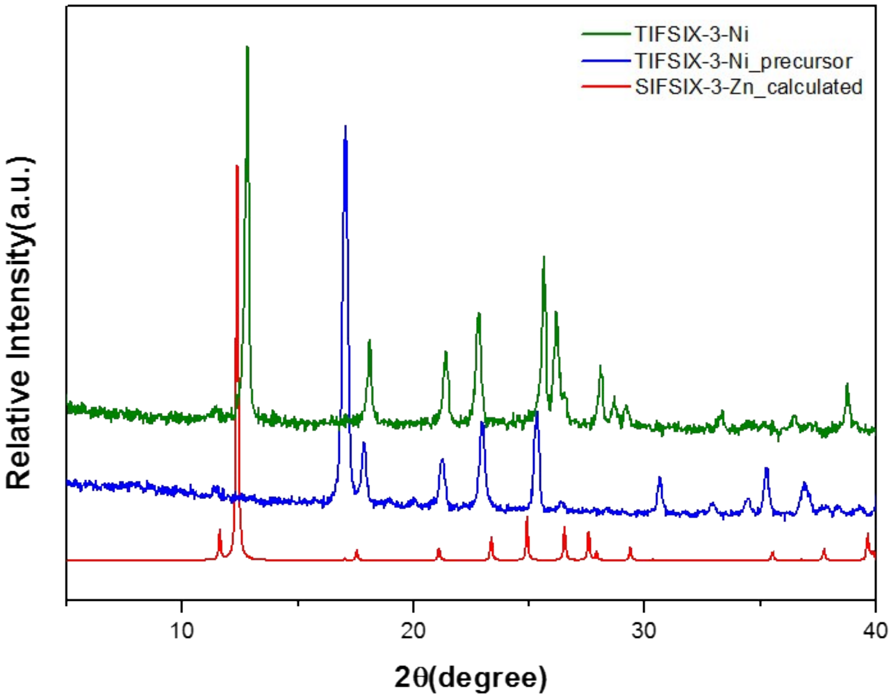

Figure S2: PXRD of **TIFSIX-3-Ni**.

Powder X-ray Diffraction for NbOFFIVE-1-Ni.

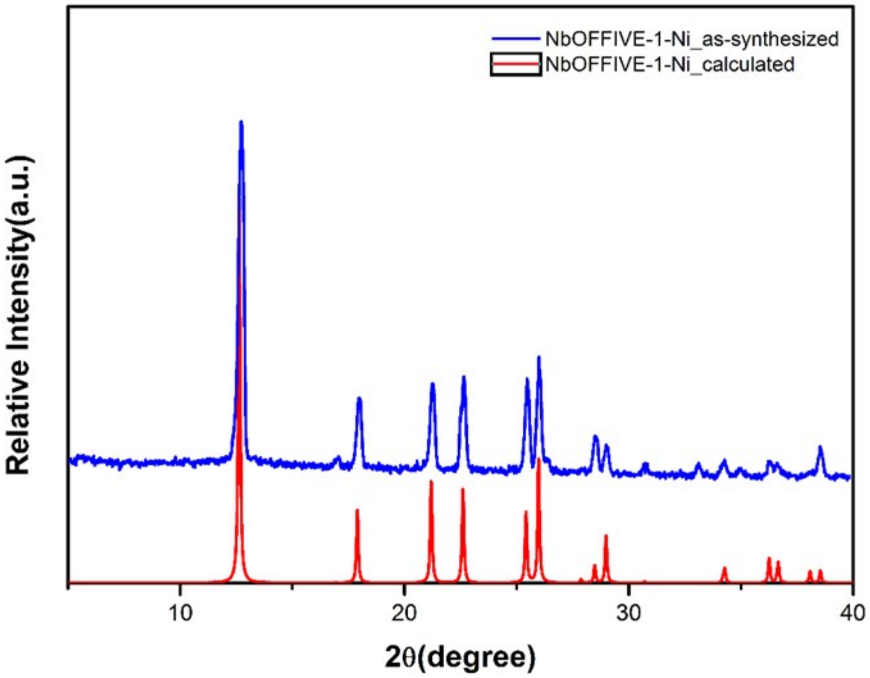

Figure S3: PXRD of **NbOFFIVE-1-Ni**.

Powder X-ray Diffraction for Mg-MOF-74.

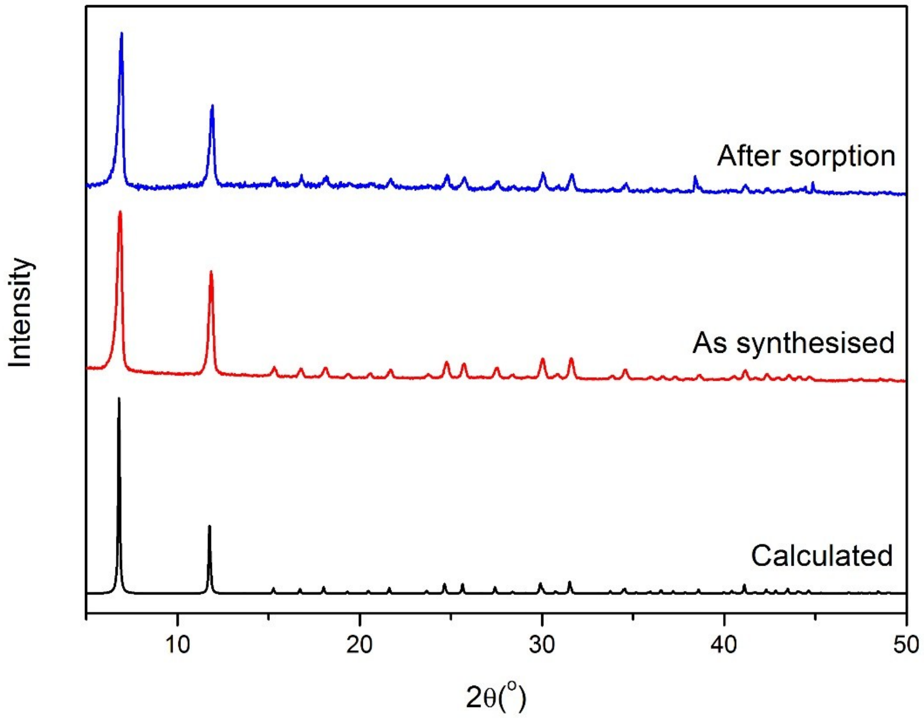

Figure S4: PXRD of **Mg-MOF-74** as synthesised and after sorption *vs*. the calculated pattern.

Powder X-ray Diffraction for UiO-66-NH$_2$.

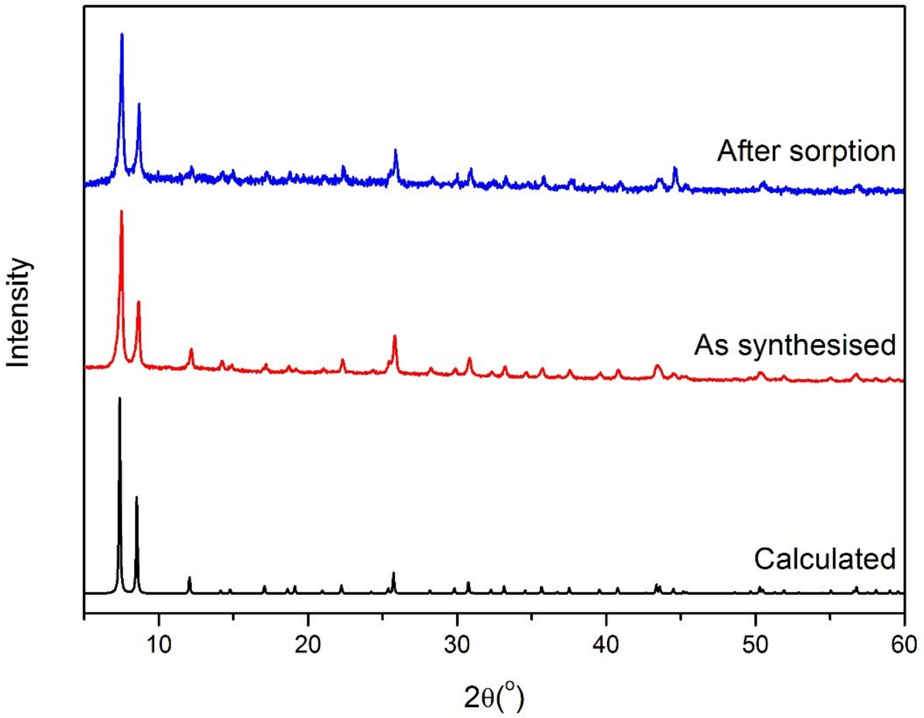

Figure S5: PXRD of **UiO-66-NH$_2$** as synthesised and after sorption *vs*. the calculated pattern.

Powder X-ray Diffraction for HKUST-1.

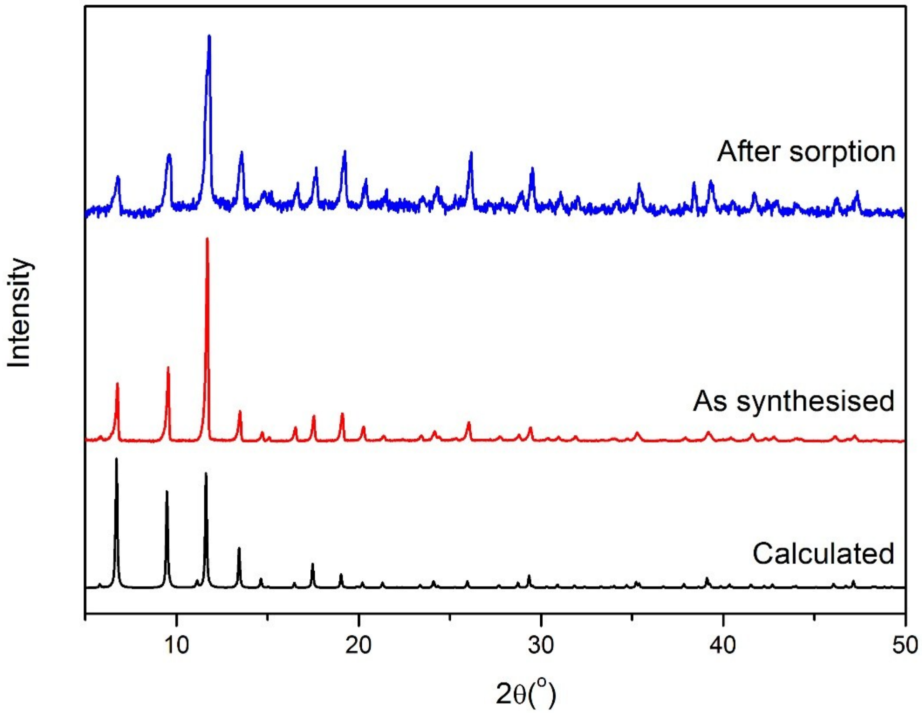

Figure S6: PXRD of **HKUST-1** as synthesised and after sorption *vs*. the calculated pattern.

Thermogravimetric Analysis for TIFSIX-3-Ni.

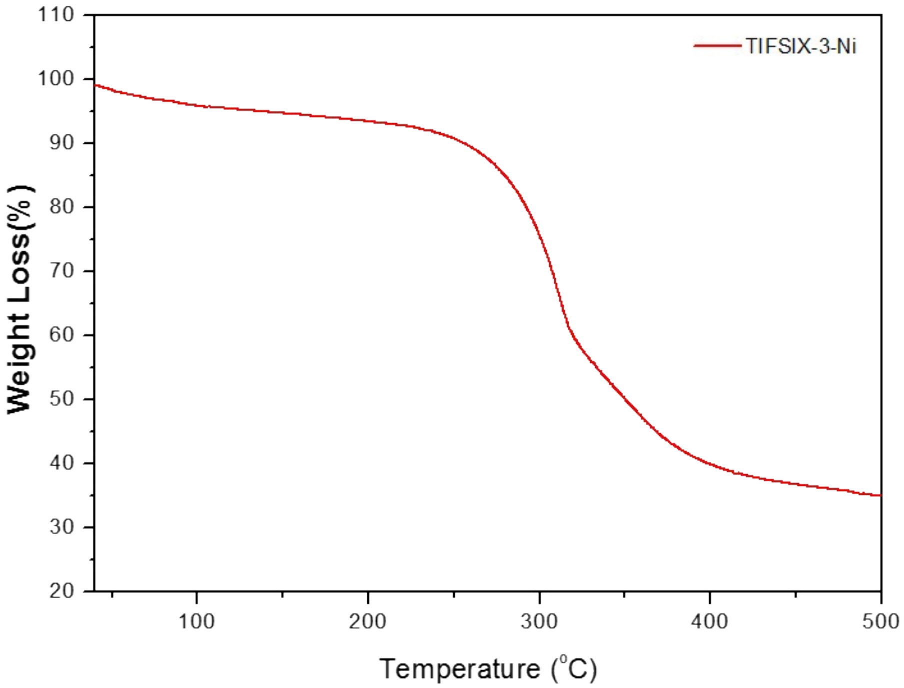

Figure S7: TGA of **TIFSIX-3-Ni**.

Thermogravimetric Analysis for NbOFFIVE-1-Ni.

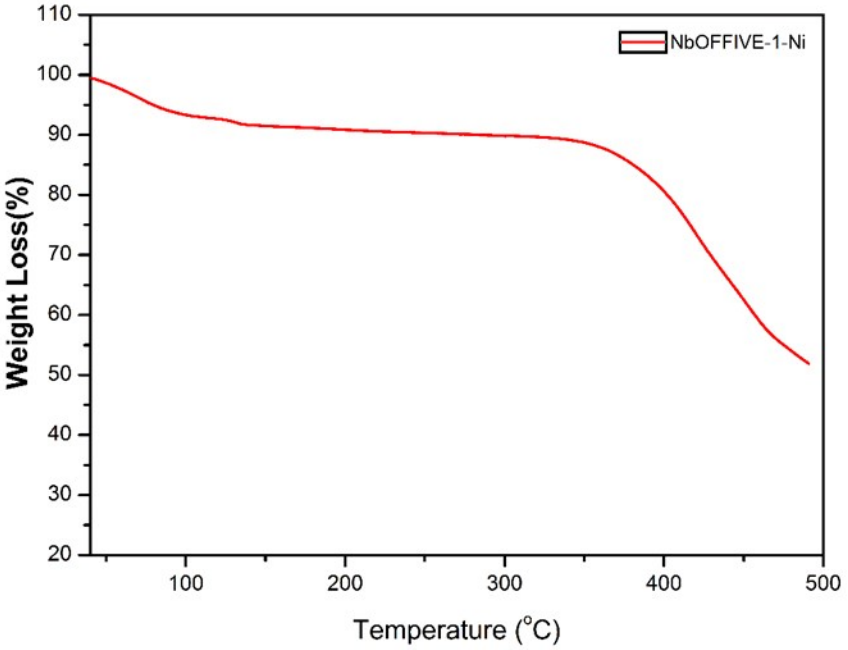

Figure S8: TGA of **NbOFFIVE-1-Ni**.

Thermogravimetric Analysis for SIFSIX-3-Ni.

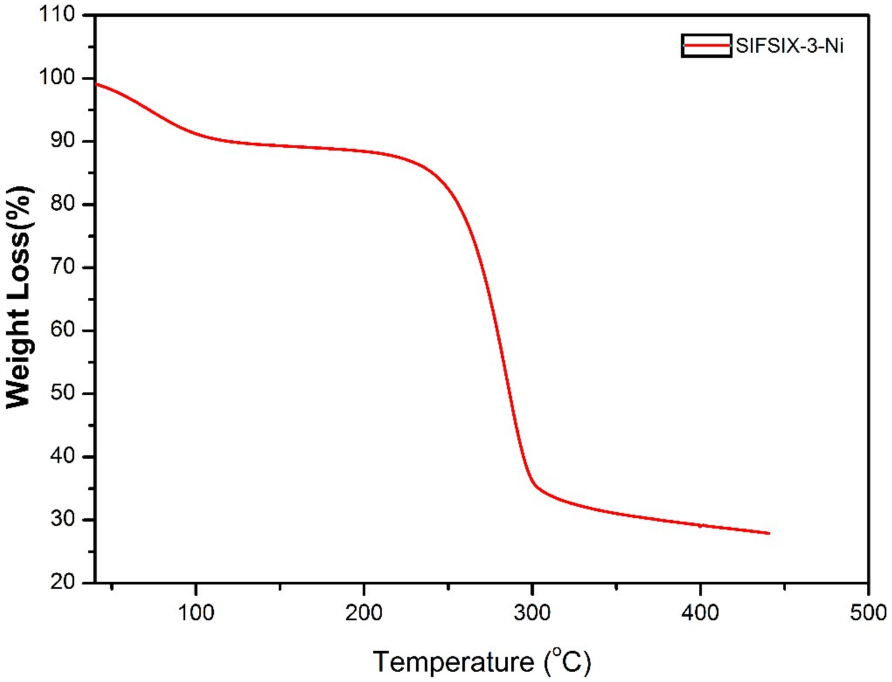

Figure S9: TGA of **SIFSIX-3-Ni**

CO_2 Sorption Isotherm for TIFSIX-3-Ni.

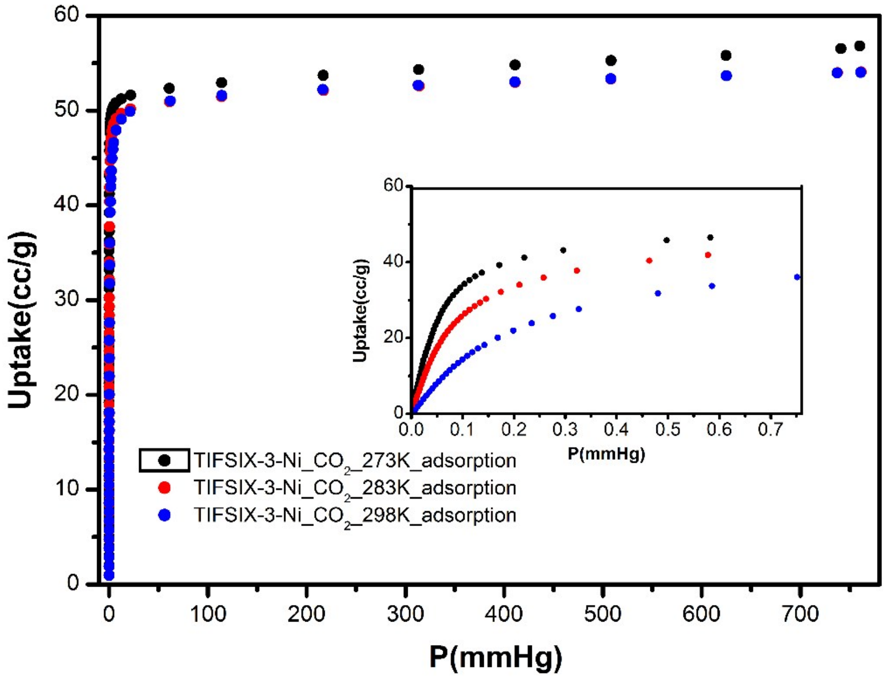

Figure S10: CO_2 sorption isotherms for **TIFSIX-3-Ni**.

CO_2 Isosteric Heat of Adsorption for TIFSIX-3-Ni.

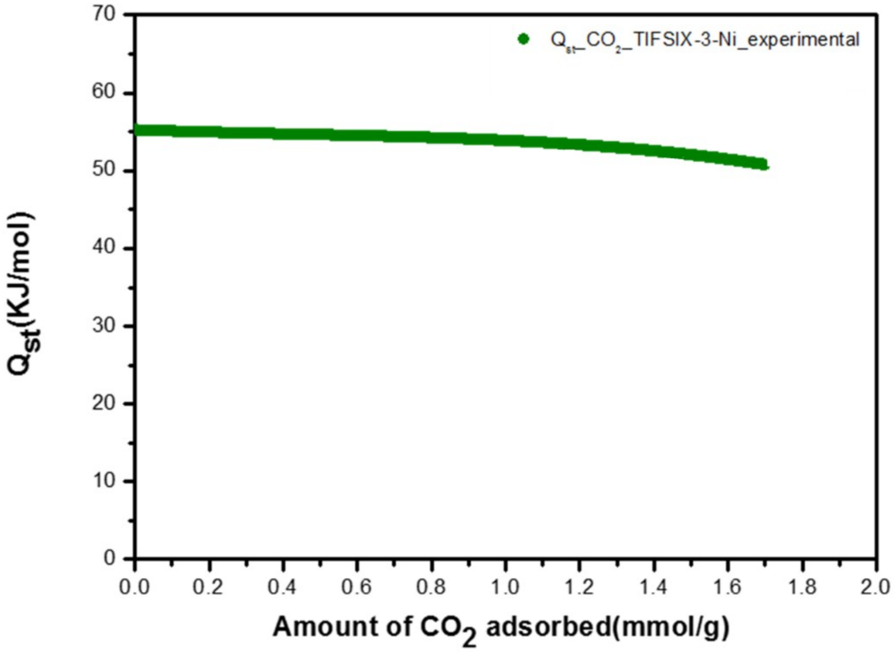

Figure S11: CO_2 isosteric heat of adsorption for **TIFSIX-3-Ni**.

Sorption Isotherms for TIFSIX-3-Ni.

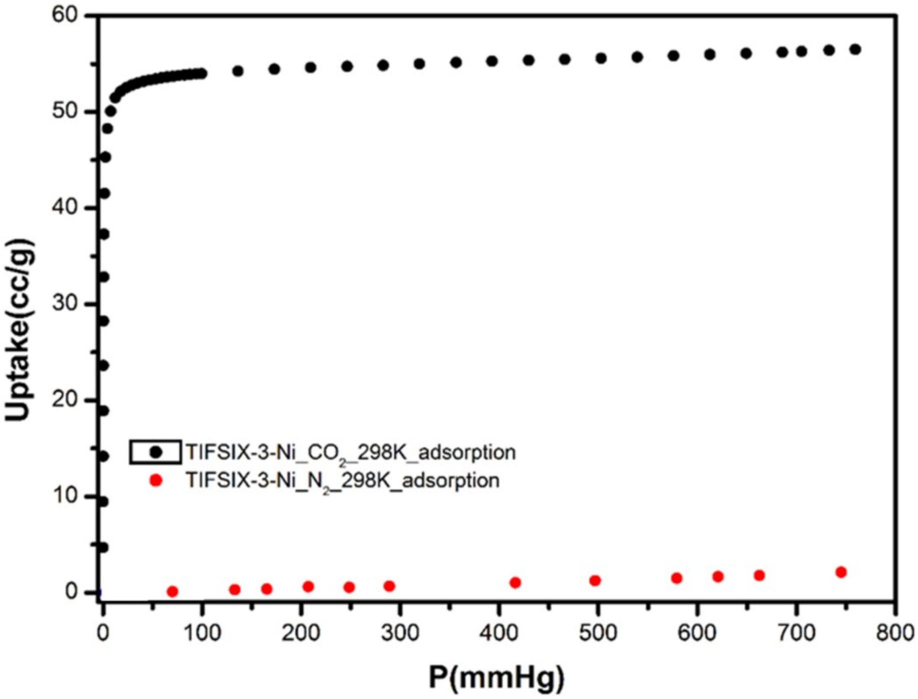

Figure S12: CO_2 (black) and N_2 (red) sorption isotherms for **TIFSIX-3-Ni**

Sorption Isotherms for NbOFFIVE-1-Ni.

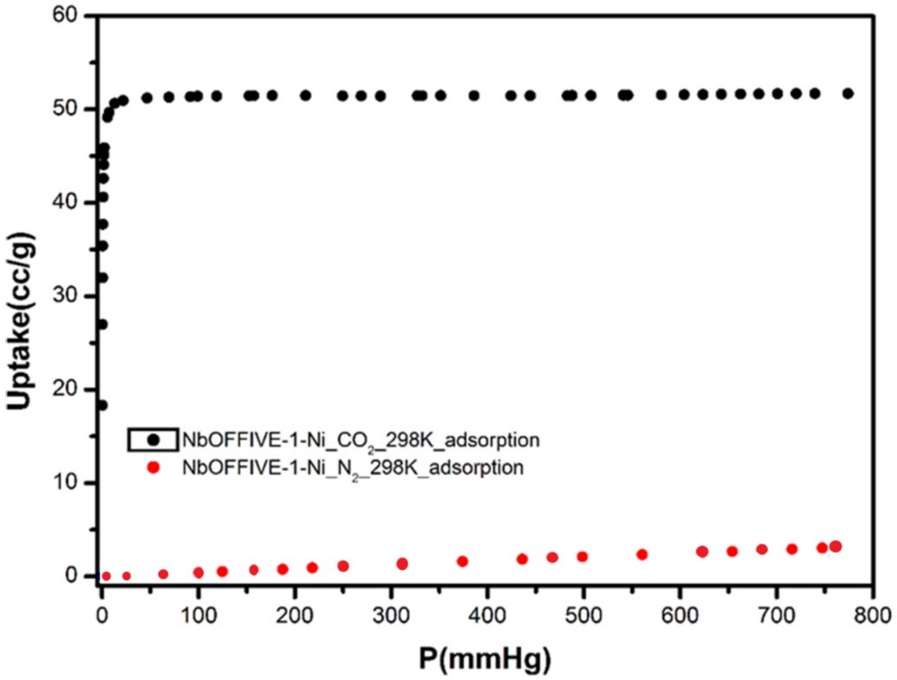

Figure S13: CO_2 (black) and N_2 (red) sorption isotherms for **NbOFFIVE-1-Ni**.

Isosteric Heats of Adsorption Calculations

The Q_{st} of CO_2 for **TIFSIX-3-Ni**, **SIFSIX-3-Ni**, **NbOFFIVE-1-Ni**, **UiO-66-NH$_2$**, **Zeolite 13X**, **HKUST-1**, **Mg-MOF-74** were calculated from the low pressure CO_2 adsorption isotherms collected at 273, 283 and 293 K.

The Clausius-Clapeyron equation was used for the calculation of Q_{st} where virial-type equations were used to fit ten points in the adsorption data between 0 and 3000 ppm (0.3 mbar) at multiple temperatures (Equation 1). The fit for each of the compounds is shown below. All fitting was performed using Origin Pro 8.

$$\ln P = \ln n + (\frac{1}{T^2})\sum_{i=0}^{j} a_i n^i + \sum_{i=0}^{k} b_i n^i$$

The Q_{st} was then calculated from the virial model using Equation 2.

$$-Q_{st} = -R\sum_{i=0}^{j} a_i n^i$$

Q_{st} Calculation - Virial Fitting for HKUST-1

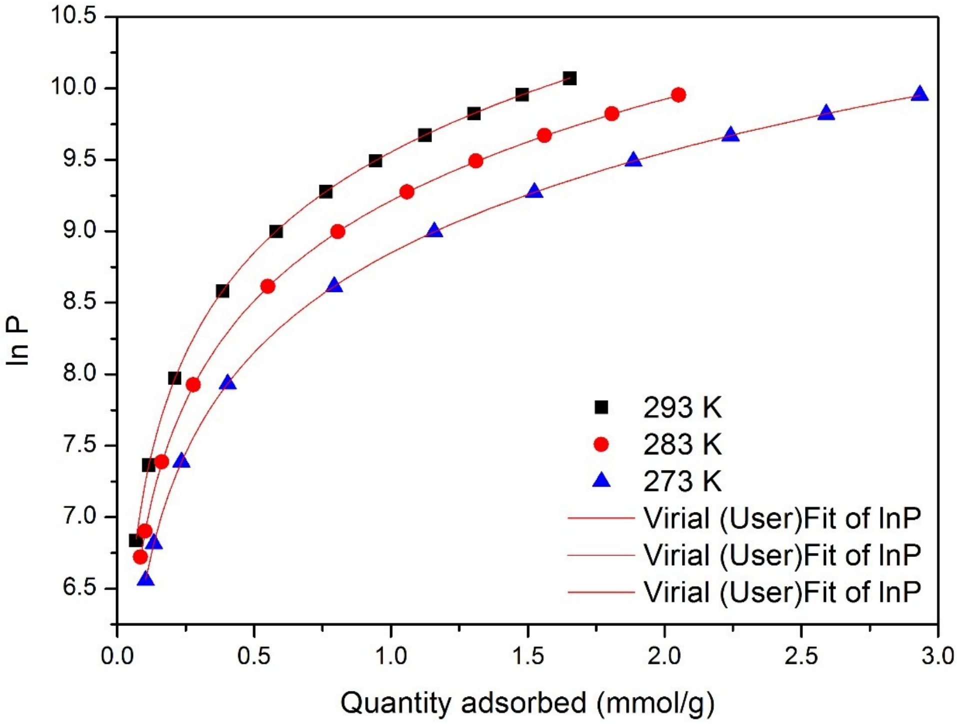

Figure S14: Fitting of the isotherm data of **HKUST-1** to the virial equation.

Table S1: Fitting parameters for **HKUST-1**.

Parameters	Value	Standard Error
a0	-2769.29899	12.84396
a1	-39.83251	13.18102
a2	-18.68377	6.89145
a3	8.48644	3.71636
a4	-1.23229	0.64041
a5	0	0
b0	18.96836	0.04548
b1	0.21259	0.04645
b2	0	0
b3	0	0
Reduced Chi-Sqr	1.77634E-5	
Adj. R-Square	0.99999	

Q_{st} Calculation - Virial Fitting for UiO-66-NH$_2$

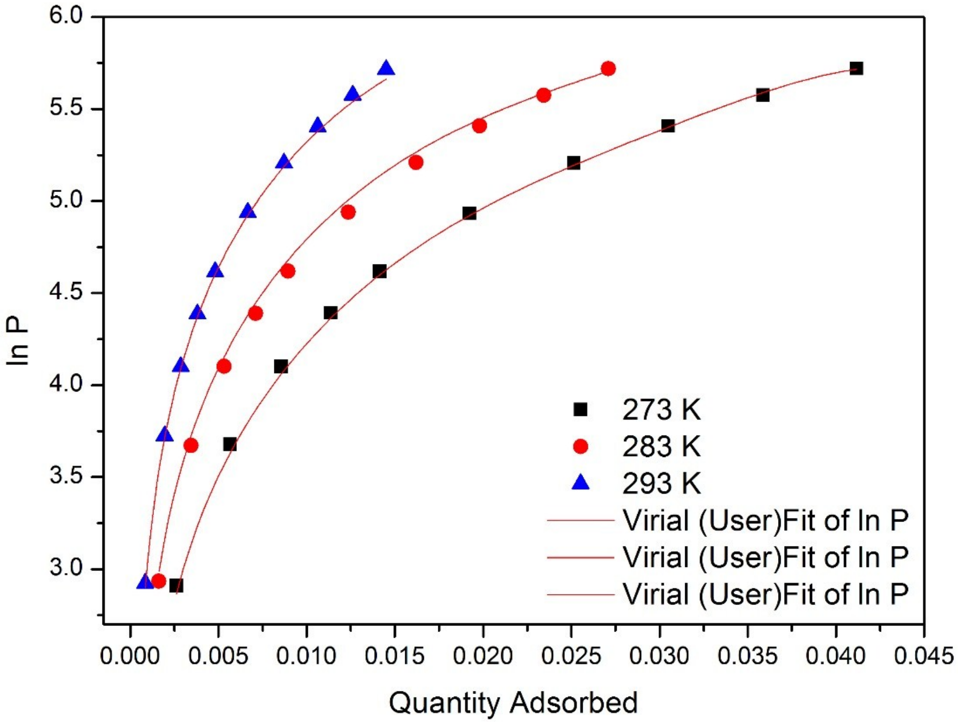

Figure S15: Fitting of the isotherm data of **UiO-66-NH$_2$** to the virial equation.

Table S2: Fitting parameters for **UiO-66-NH$_2$**.

Parameters	Value	Standard Error
a0	-4652.39339	134.02036
a1	651.0126	491.60026
a2	-636.66509	429.18299
a3	224.05882	105.79837
a4	-0.95913	2.45873
a5	0	0
b0	25.81332	0.463
b1	-1.82217	1.6815
b2	2.23851	1.43952
b3	-0.79225	0.33345
Reduced Chi-Sqr	0.00231	
Adj. R-Square	0.99941	

Q_{st} Calculation - Virial Fitting for Mg-MOF-74

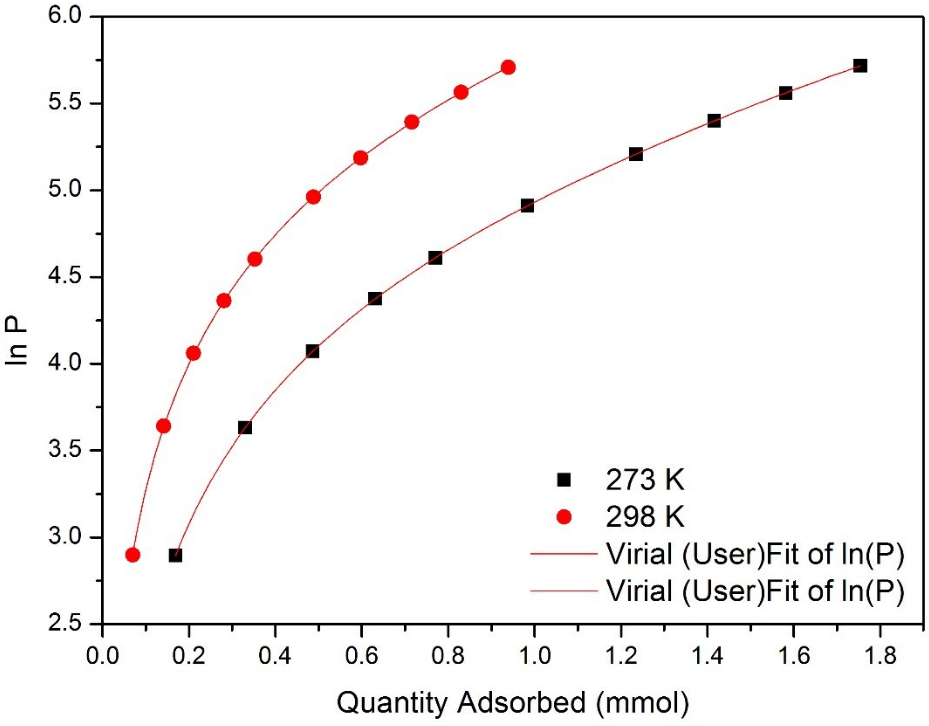

Figure S16: Fitting of the isotherm data of **Mg-MOF-74** to the virial equation.

Table S3: Fitting parameters for **Mg-MOF-74**.

Parameters	Value	Standard Error
a0	-5097.16475	18.97529
a1	574.65484	82.27637
a2	-321.76928	83.09131
a3	82.79407	17.78506
a4	-17.52221	4.63194
a5	0	0
b0	15.93129	0.06358
b1	-1.50837	0.26696
b2	0.68876	0.23788
b3	0	0
Reduced Chi-Sqr	6.37182E-6	
Adj. R-Square	0.99999	

Q_{st} Calculation - Virial Fitting for Zeolite 13X

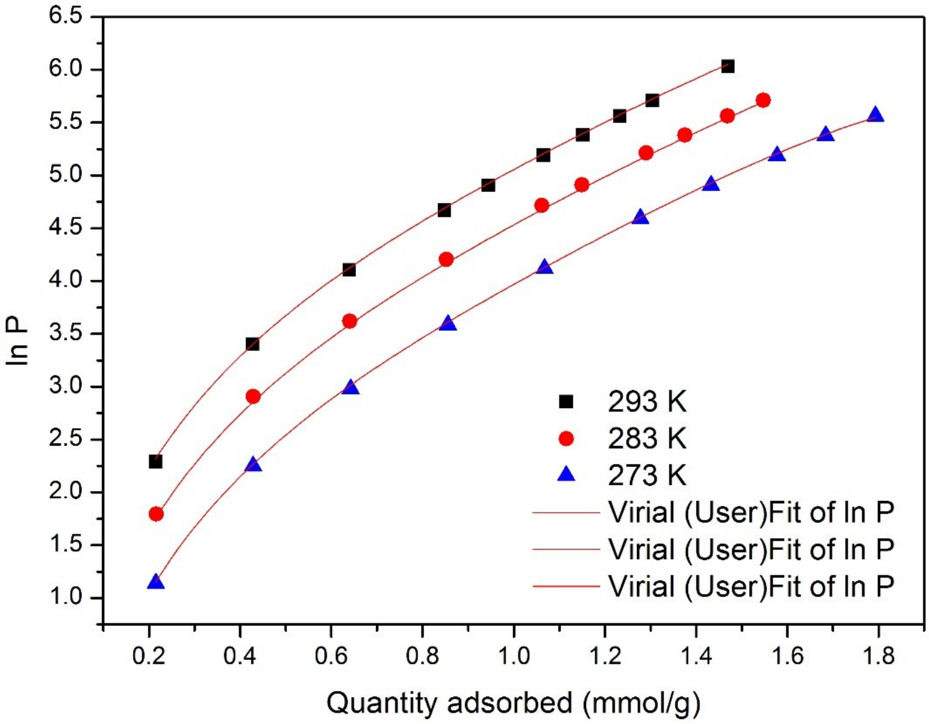

Figure S17: Fitting of the isotherm data of **Zeolite 13X** to the virial equation.

Table S4: Fitting parameters for **Zeolite 13X**.

Parameters	Value	Standard Error
a0	-4800.00613	132.39722
a1	797.61373	176.85271
a2	-676.20166	219.18557
a3	433.94642	160.8827
a4	-104.16306	40.50343
a5	0	0
b0	19.70324	0.46117
b1	0.19534	0.45833
b2	0	0
b3	0	0
Reduced Chi-Sqr	7.78166E-4	
Adj. R-Square	0.99954	

Q_{st} Calculation - Virial Fitting for SIFSIX-3-Ni

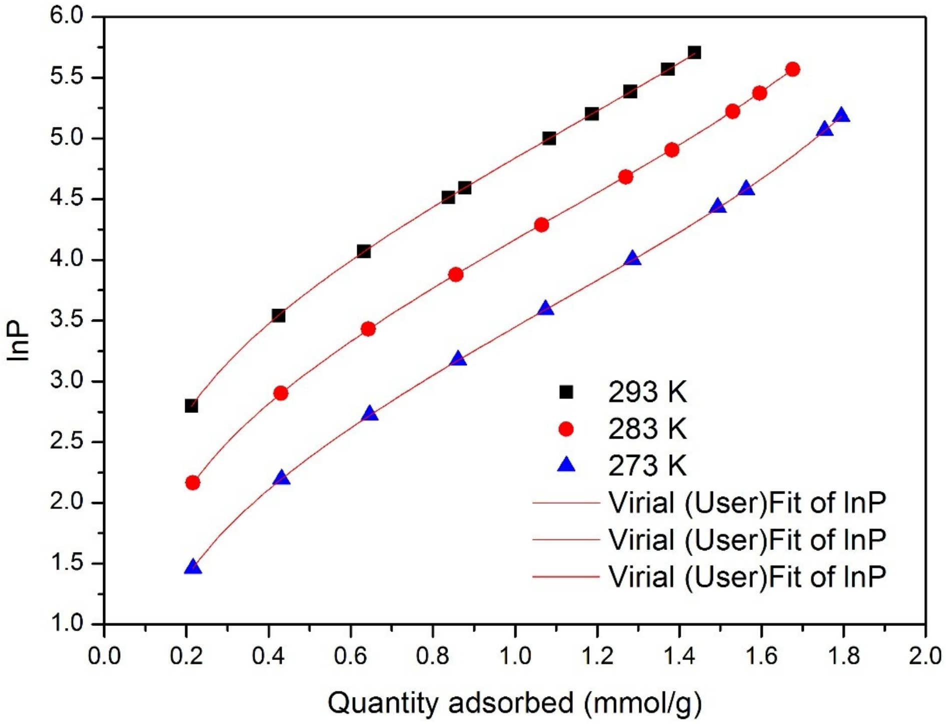

Figure S18: Fitting of the isotherm data of **SIFSIX-3-Ni** to the virial equation.

Table S5: Fitting parameters for **SIFSIX-3-Ni**.

Parameters	Value	Standard Error
a0	-5275.96689	35.74562
a1	-658.17726	87.8135
a2	639.49304	52.52675
a3	-367.67605	26.83061
a4	99.0502	6.83313
a5	0	0
b0	22.41777	0.1273
b1	1.56213	0.31722
b2	-0.15424	0.17365
b3	0	0
Reduced Chi-Sqr	1.94117E-5	
Adj. R-Square	0.99999	

Q_{st} Calculation - Virial Fitting for TIFSIX-3-Ni

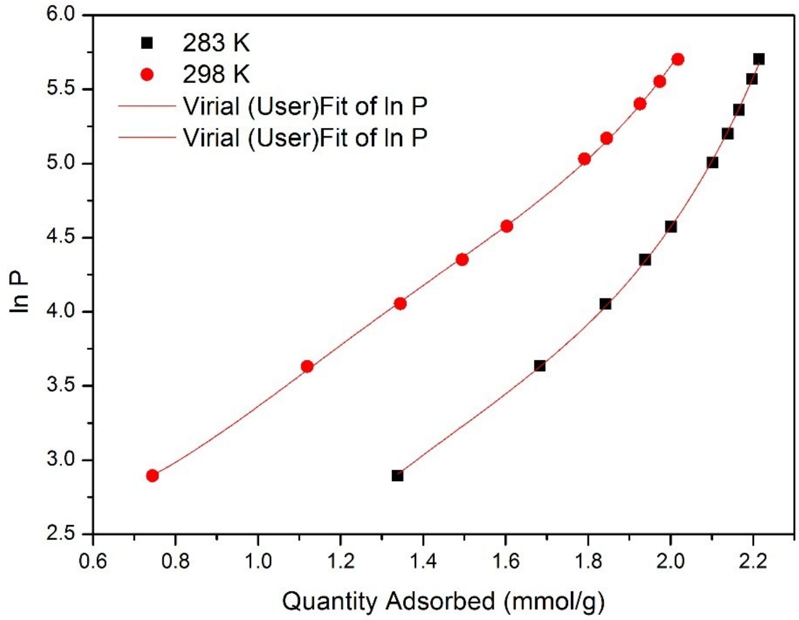

Figure S19: Fitting of the isotherm data of **TIFSIX-3-Ni** to the virial equation.

Table S6: Fitting parameters for **TIFSIX-3-Ni**.

Parameters	Value	Standard Error
a0	-5643.77909	233.09913
a1	-3582.12507	699.32213
a2	4493.99446	749.85233
a3	-2281.59589	340.83247
a4	436.56659	55.92704
a5	0	0
b0	25.43248	0.18808
b1	0	0
b2	0	0
b3	0	0
Reduced Chi-Sqr	3.15597E-4	
Adj. R-Square	0.9996	

DAC TPD for TIFSIX-3-Ni.

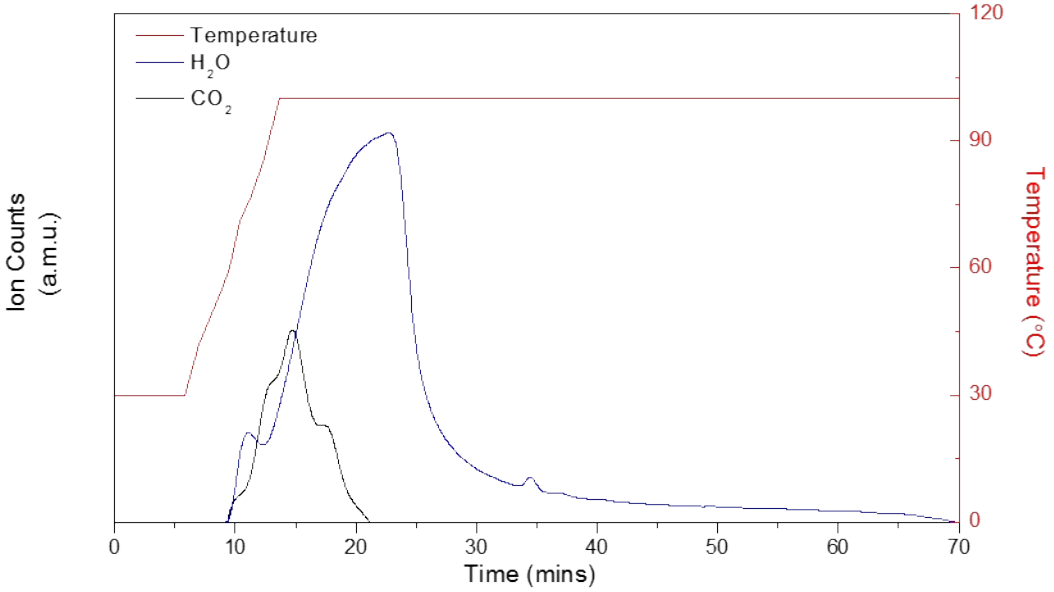

Figure S20: DAC test TPD for **TIFSIX-3-Ni**

DAC TPD for NbOFFIVE-1-Ni.

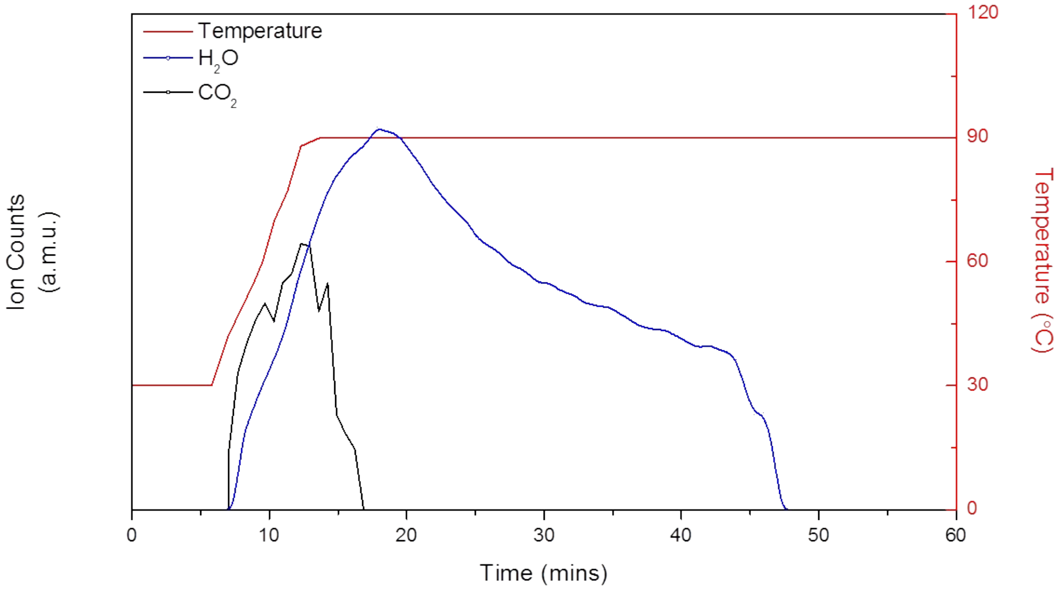

Figure S21: DAC test TPD for **NbOFFIVE-1-Ni**

Accelerated Stability Test for TIFSIX-3-Ni.

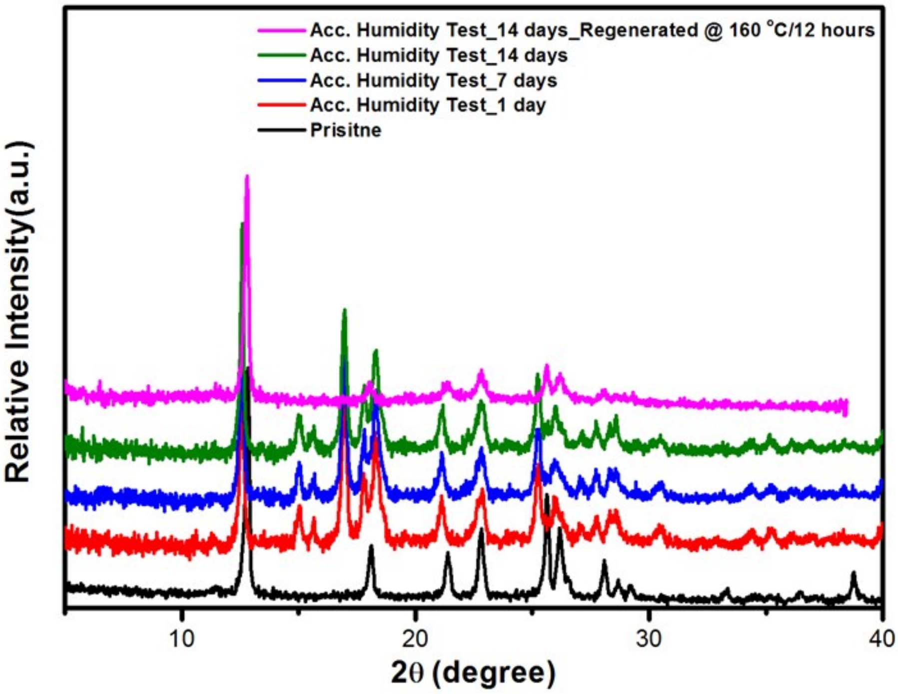

Figure S22: PXRD for **TIFSIX-3-Ni** after accelerated stability test.

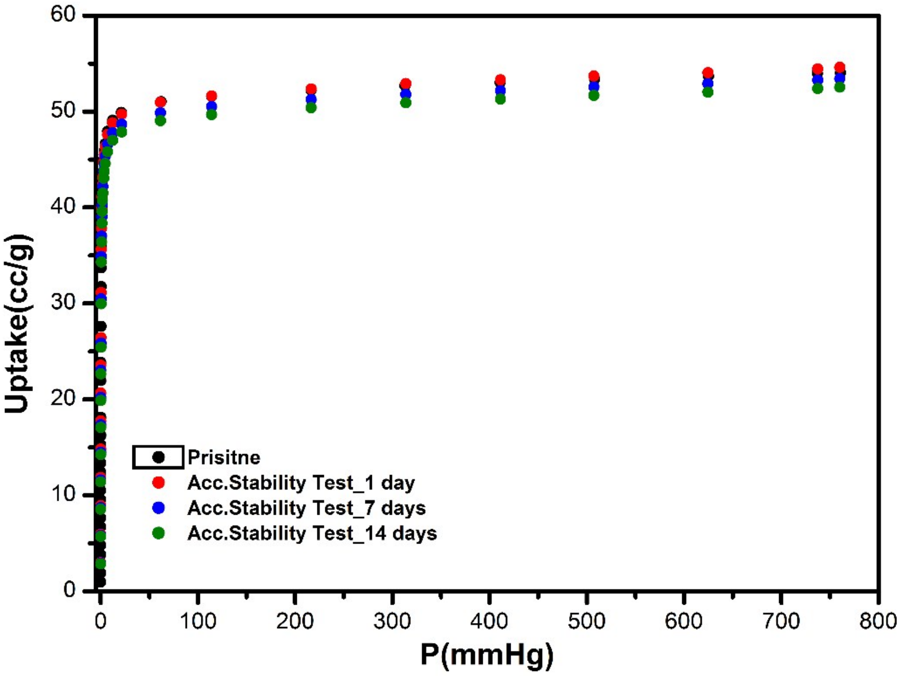

Figure S23: Sorption for **TIFSIX-3-Ni** after accelerated stability test.

Accelerated Stability Test for NbOFFIVE-1-Ni.

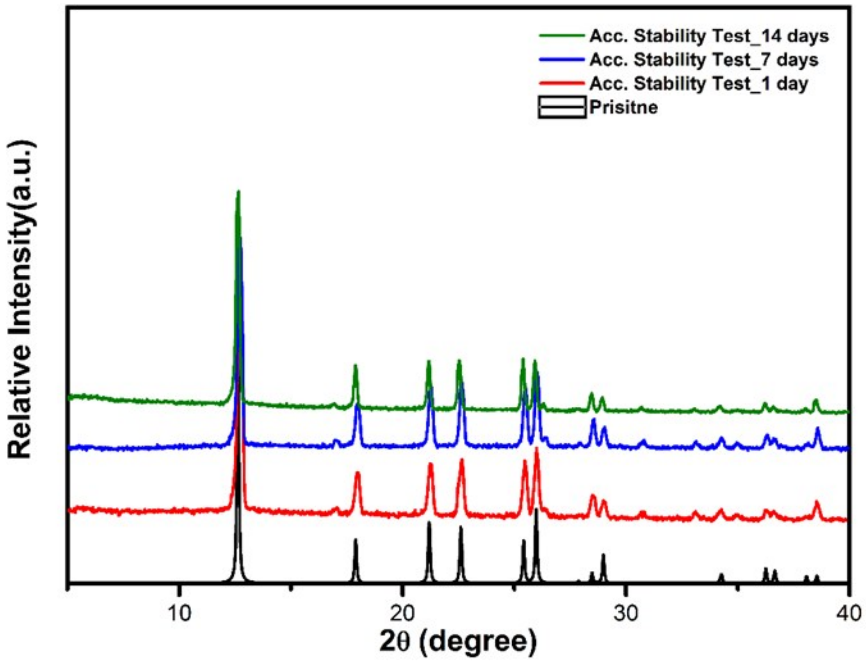

Figure S24: PXRD for **NbOFFIVE-1-Ni** after accelerated stability test.

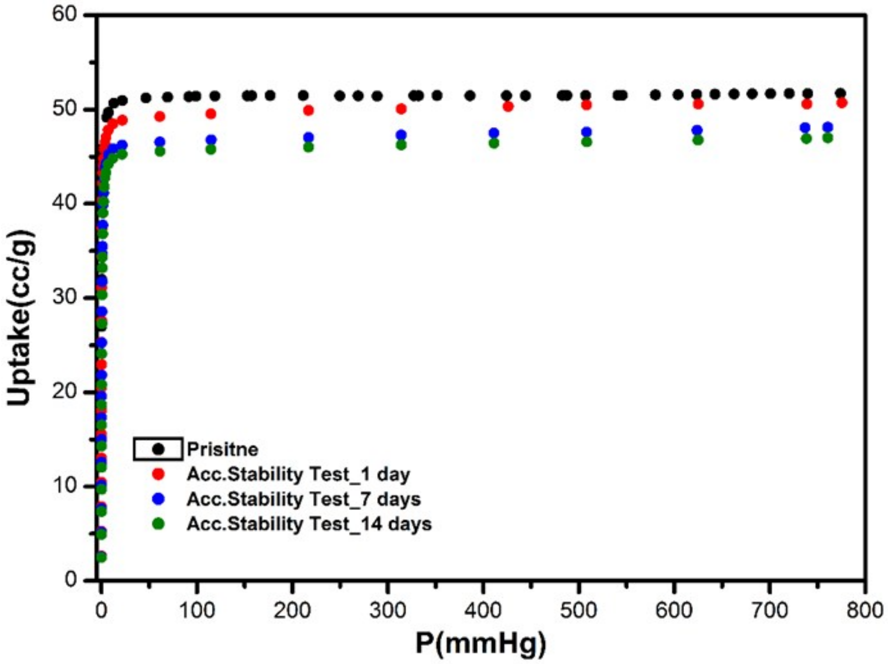

Figure S25: Sorption for **NbOFFIVE-1-Ni** after accelerated stability test.

VT-PXRD for TIFSIX-3-Ni.

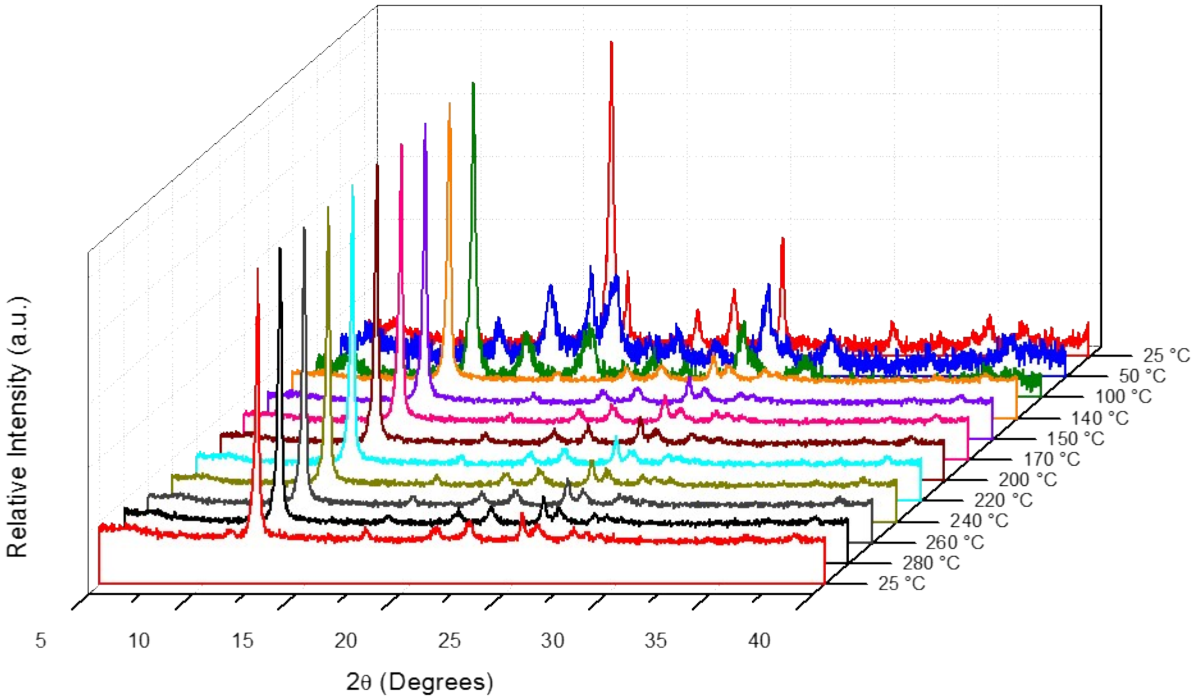

Figure S26: VT-PXRD of **TIFSIX-3-Ni. This series of diffractograms shows the temperature-induced transformation {rear to front} of the precursor (red: 25 °C) into TIFSIX-3-Ni (orange: 140 °C).**

VT-PXRD for SIFSIX-3-Ni.

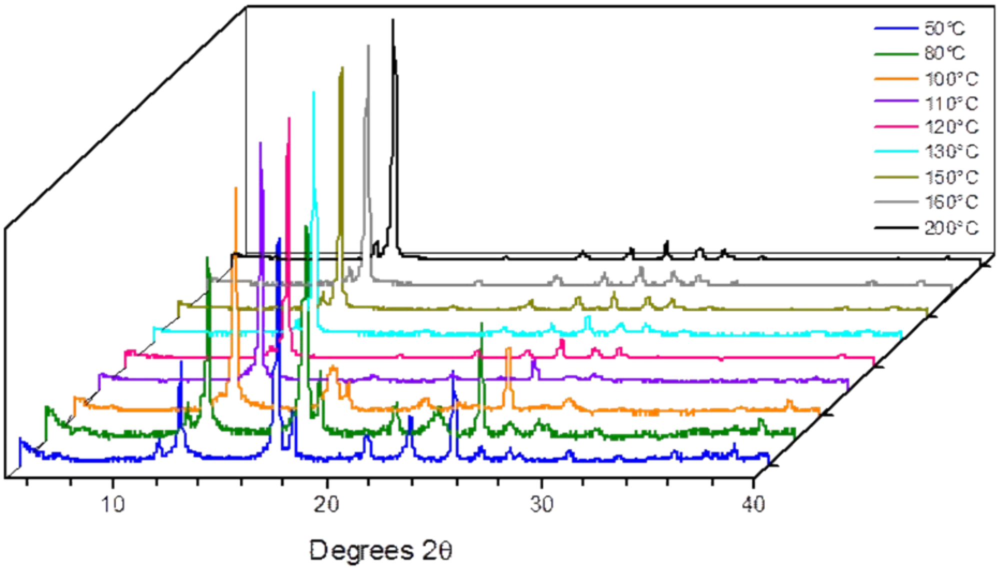

Figure S27: VT-PXRD of **SIFSIX-3-Ni.**

Rietveld Fitting of the PXRD Pattern for TIFSIX-3-Ni.

Powder diffraction data used for structure solution was obtained from beamline i11 at the Diamond Light Source (λ = 0.82620(6) and zero point = -0.0367(1)).[9] Due to the high energy X-ray source, two second scans using a positional scanning detector was used to collect data from a powder sample sealed in a 0.6 mm quartz capillary tube. Analysis of the powder data was carried out in GSAS-II;[10] the lattice parameters were determined and structure factors obtained by use of the Pawley method. A Monte Carlo/simulated annealing method was used for structure solution using free moving rigid bodies obtained from the Cambridge Structural Database (CSD)[11] (CSD refcode: PETWIW = TiF_6, AHADUI = pyrazine). (See **Table S7** for crystallographic details).

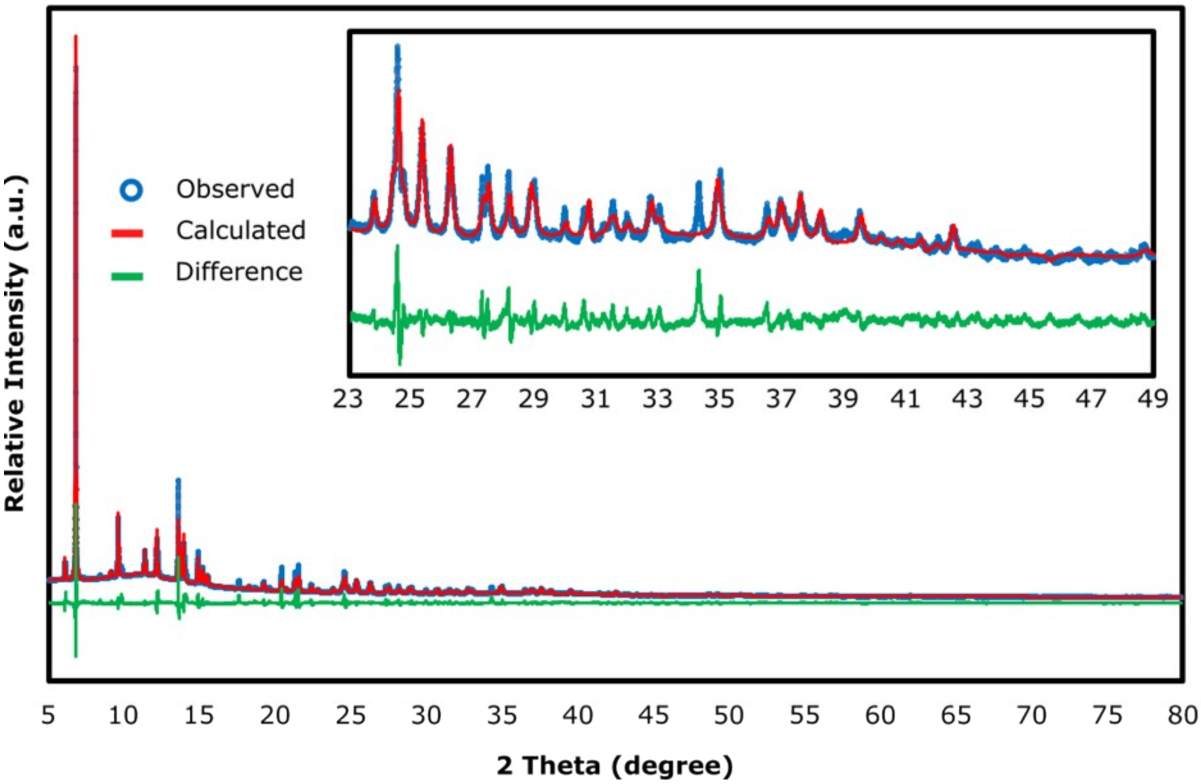

Figure S28: Diffractograms for the Rietveld refinement of **TIFSIX-3-Ni**. Inset depicts a more detailed view of the high angle data (2Å < *d* < 1Å)

Table S7: Crystallographic data for TIFSIX-3-Ni

Spacegroup	***P*4/*mmm***
a (Å)	**6.99007(18)**
c (Å)	**7.81267(21)**
V (Å^3)	**381.735(15)**
R_{p}	**0.04482**
R_{wp}	**0.07356**
R_{bragg}	**0.09798**
R_{exp}	**0.01609**
Goodness-of-fit	**4.58**

References.

1 S. K. Elsaidi, M. H. Mohamed, H. T. Schaef, A. Kumar, M. Lusi, T. Pham, K. A. Forrest, B. Space, W. Xu, G. J. Halder, J. Liu, M. J. Zaworotko, P. K. Thallapally, *Chem. Commun. (Cambridge, U. K.)* 2015, **51**, 15530.

2 S. R. Caskey, A. G. Wong-Foy, A. J. Matzger, *J. Am. Chem. Soc.* 2008, **130**, 10870.

3 S. J. Garibay, S. M. Cohen, *Chem. Commun. (Cambridge, U. K.)* 2010, **46**, 7700.

4 P. D. C. Dietzel, B. Panella, M. Hirscher, R. Blom, H. Fjellvag, *Chem. Commun. (Cambridge, U. K.)* 2006, 959.

5 F. Raganati, V. Gargiulo, P. Ammendola, M. Alfe, R. Chirone, *Chem. Eng. J. (Lausanne)* 2014, **239**, 75.

6 A. Cadiau, K. Adil, P. Bhatt, Y. Belmabkhout, M. Eddaoudi, *Science* 2016, **353**, 137.

7 I. H. T. Guideline, *Q1A (R2), current step* 2003, **4**.

8 K. C. Waterman, in *Handbook of stability testing in pharmaceutical development*, Springer, **2009**, pp. 115.

9 C. Tang, S. Thompson, T. Hill, G. Wilkin, U. Wagner, *Zeitschrift fur Kristallographie Supplements* 2007, **2007**, 153.

10 B. H. Toby, R. B. Von Dreele, *J. Appl. Crystallogr.* 2013, **46**, 544.

11 C. R. Groom, I. J. Bruno, M. P. Lightfoot, S. C. Ward, *Acta Crystallographica Section B: Structural Science, Crystal Engineering and Materials* 2016, **72**, 171.